LA-UR- 10-00734

Approved for public release; distribution is unlimited.

Title: Ejecta Model Development at pRad (U)

Author(s): W. T. Buttler, D. M. Oro, G. Dimonte, C. Morris, G. Terrones, J. R. Bainbridge, G. E. Hogan, B. Hollander, D. Holtkamp, K. Kwiatkowski, M. Marr-Lyon, F. Mariam, F. E. Merrill, P. Nedrow, A. Saunders, C. L. Schwartz, B. Stone, D. Tupa, and W. S. Vogan-McNeil

Intended for: Proceedings NEDPC 2009

Los Alamos
NATIONAL LABORATORY
EST. 1943

Los Alamos National Laboratory, an affirmative action/equal opportunity employer, is operated by the Los Alamos National Security, LLC for the National Nuclear Security Administration of the U.S. Department of Energy under contract DE-AC52-06NA25396. By acceptance of this article, the publisher recognizes that the U.S. Government retains a nonexclusive, royalty-free license to publish or reproduce the published form of this contribution, or to allow others to do so, for U.S. Government purposes. Los Alamos National Laboratory requests that the publisher identify this article as work performed under the auspices of the U.S. Department of Energy. Los Alamos National Laboratory strongly supports academic freedom and a researcher's right to publish; as an institution, however, the Laboratory does not endorse the viewpoint of a publication or guarantee its technical correctness.

Form 836 (7/06)

Ejecta Model Development at pRad (U)

W. T. Buttler, D. M. Oro, G. Dimonte, C. Morris, G. Terrones, J. R. Bainbridge, G. E. Hogan, B. Hollander, D. Holtkamp, K. Kwiatkowski, M. Marr-Lyon, F. Mariam, F. E. Merrill, P. Nedrow, A. Saunders, C. L. Schwartz, B. Stone, D. Tupa, and W. S. Vogan-McNeil

Los Alamos National Laboratory, Los Alamos, New Mexico

In July 2009 we fielded three explosively (HE) driven Richtmyer-Meshkov instability experiments at the LANSCE Proton Radiography Facility (pRad), and in August of 2009 we fielded one flyer plate experiment on the pRad 40 mm powder gun. One HE experiment was done in vacuum, and the other two within four atmospheres of noble gasses: Xe and Ne. These two gasses were chosen to study the viscous effects on ejecta formation. It is unexpected, but the viscosity η of Ne is twice that of Xe, and, due to the atomic mass difference between the two, the kinematic viscosity (η/ρ) of Ne is about ten times that of Xe. The results showed that ejecta formation is sensitively linked to the gas density, which implies that the Weber number is more important in ejecta formation than the Reynolds number.

Los Alamos National Laboratory (LANL) is presently engaged in development and implementation of ejecta source term and transport models for integration into LANL hydrodynamic computer codes. Support of that effort spans a broad array of experimental activities, including gun- and HE-driven ejecta source and transport measurements from machine roughened Sn surfaces.[1-9] Because the underlying postulate for ejecta formation is that ejecta are characterized by a special limiting case of a Richtmyer-Meshkov instability (RMI),[10,11] where the Atwood number is $A = -1$,[12] a key element of the source modeling and transport centers on shocked-Sn validation and verification RMI experiments, such as the experimental results presented here.

In past LANL RMI experiments, the instabilities were formed by shocking the Sn with a high speed flyer launched fast enough to liquify the Sn on shock. However, because most of our roughened surface ejecta data come from HE shocked Sn samples,[13] we altered the FY09 experiments to include HE driven measurements. This change in philosophy required a quick experimental package redesign to facilitate a success oriented schedule. The redesign was further complicated because the Sn HE ejecta experiments were typically done at shock pressures just prior to release of $P_{SB} \leq 30.0$ GPa. Our initial estimates of the pressures concluded that the pressures for these experiments would be closer to $P_{SB} \approx 35$ GPa, which was confirmed by velocity measurements effected with optical Doppler velocimetry methods, as well as velocity estimates from the proton radiographs.

It is important to note that the FY09 experimental package designs were informed by FY08 activities. In FY08, our Forest flyer[14] plate-impact experiments were done at pRad with the $-I$ magnetic lens: one experiment in vacuum and one in gas. On those experiments the flyer velocity was diagnosed with proton radiograph images of the flyer in flight. This flyer plate velocity was then used to estimate the material loading pressure,[15] which typically turned out to be $P_{SB} \geq 65$ GPa. These pressures are, technically, too high to study the ejecta formation as the Sn liquifies on shock at these pressures. The HE geometry lowered this pressure, but it nevertheless remains high relative to the lower pressures we want to achieve in FY10, which are more commensurate with the roughened surface ejecta studies that have loading pressures prior to release of $16 \leq P_{SB} \leq 30$ GPa. The implication is that the FY10 packages must be redesigned to achieve these lower pressures, or else different materials, such as Cu, will need to be studied. Further, the late-time curvature of our dynamic system complicates hydrodynamic studies of the RMI phenomena. Therefore, designs that minimize curvature caused by release waves are

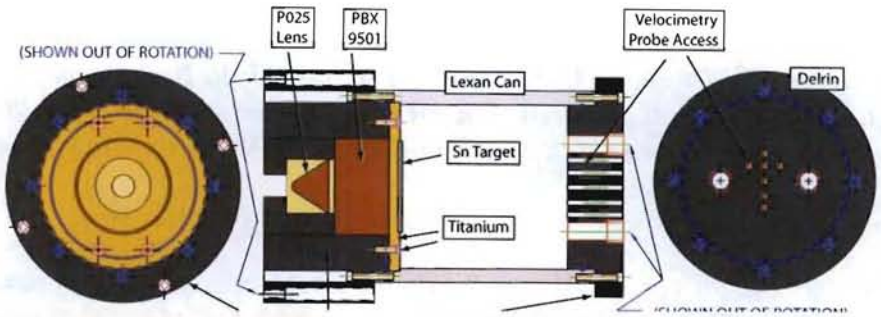

Fig. 1 This figure shows the HE package geometry together with the pressure can assembly.

sought, with HE systems or otherwise.

The FY09 package design is presented in Fig. 1, with individual components shown in Fig. 2. This package incorporated a P025 HE lens and a PBX 9501 booster in contact with the titanium buffer onto which the Sn sample was mounted. The HE was confined within a Delrin cylinder that had a Lexan tube capped by Delrin. The Delrin cap further permitted inclusion of seven laser Doppler velocimetry probes that were positioned to monitor the free surface velocity in four places, and the RMI bubble and spike velocities. (These experiments were the first experiments in which the bubble and spike velocities were monitored relative to the particle velocity.) Monitoring of the particle velocimetry relates the shockwave loading pressure just prior to release, and the monitoring of the RMI bubble and spike velocity gives the nonlinear regime of the bubble and spike velocity growth together with the saturation velocities of each.

The Ti buffer had an outer diameter, $d = 76.2$ mm and thickness, $\tau = 4$ mm, with a 1 mm deep counter-sunk area, on the package center-line, that was cut to the Sn target diameter of $d = 42$ mm. The Sn target was epoxied into the counter-sunk region. The average Sn target thickness was $\tau = 2$ mm, and had three regions with a sine-wave pattern machined into the surface. The three regions were separated by two flat regions used to determine the shocked surface particle velocity. The three sine-wave areas were defined by two different wavelengths of $\lambda_1 = 0.60$ mm, $\lambda_2 = 2.5$ mm, and $\lambda_3 = 0.60$ mm. The corresponding sine-wave amplitudes were $a_1 = 0.025$ mm, $a_2 = 0.10$ mm, and $a_3 = 0.10$ mm. These

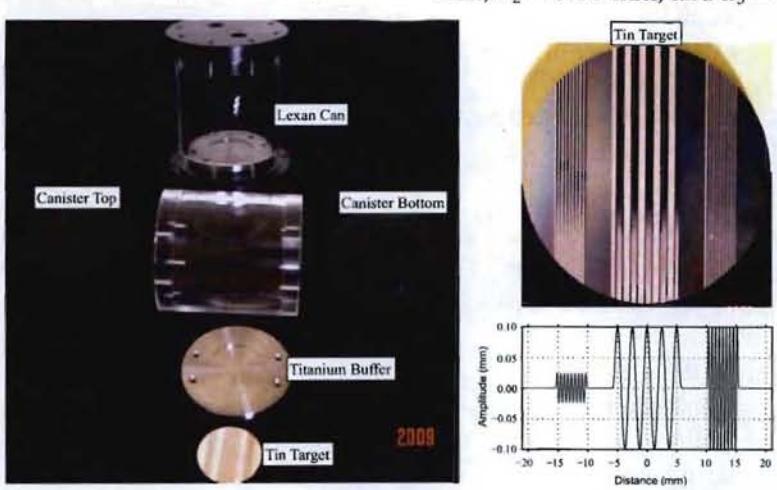

Fig. 2. Target package parts for the FY09 RMI experimental series. The targets included the three sine-wave regions separated by two flat regions finished to R_a = 16 μin. (0.4 μm) roughness across the surface, including the sine-wave regions. This roughened finish can be seen in the target photograph on the upper right.

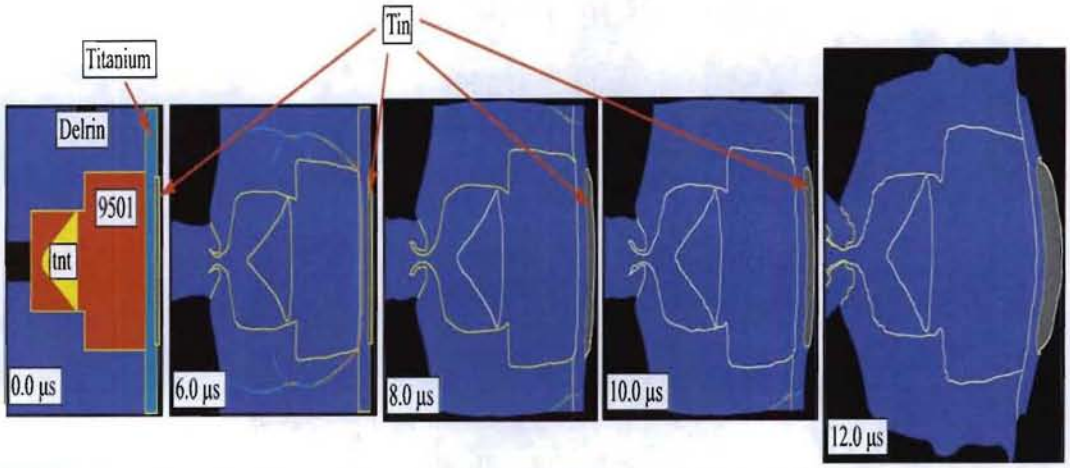

Fig. 3. Hydrodynamic modeling results for the Fig. 1 experimental package design. In these images, the left image shows the TNT, Delrin, PBX 9501, Ti and Sn locations. Subsequent images show the outlines of the expanded product locations in yellow, with the Sn in solid gray. The shockwaves are also shown as they transmit and reflect within the shocked, expanding materials. The Sn is seen to decompress with time.

parameters gave wave-number and amplitude products of $k_1\, a_1 = k_2\, a_2 = 1/4$, and $k_3\, a_3 = 1$.

Figure 2 includes photographs of the Fig. 1 parts together with a photograph of one of the Sn targets and a cross-section view of the requested finish. Embedded on top of the otherwise smooth finish was a machine roughness of $R_a = 16$ µin. (0.4 µm). Future experiments will require a diamond-turned finish as ejecta from this roughness was seen above the shocked surfaces in the pRad radiographs. Earlier ejecta studies have shown that diamond turned finishes produce essentially no ejecta, which is consistent with RMI theory of long-wavelength and small-amplitude perturbations.

The hydrodynamics for the Fig. 1 experimental package were modeled with Pagosa in X-4. The modeled results are shown in Fig. 3. The times on the lower left are relative to detonator breakout. The materials are identified within the figures: Delrin, TNT, PBX 9501, the Ti buffer, and the Sn target. A close inspection of the calculation shows the shockwaves in the Delrin, Ti, and the reflected shockwaves from the Ti back into the HE byproducts.

The goal of the hydrodynamic modeling is to determine if the package curvature can be modeled well, and once done, to use the modeling to inform future package designs. Not shown in the modeling results of Fig. 3 is the Lexan can that was used to pressurize the package with Ne and Xe for two of the experiments. In those two experiments, the gas pressure was 4 atm., for each experiment. Therefore, for this RMI experimental series we fielded three packages: vacuum, 4 atm. Xe, and 4 atm. Ne. The Ne and Xe experiments studied the effects of viscosity versus gas density on spike breakup, or ejecta transport.

In fielding experiments, at pRad it is necessary to establish the type of imaging experiment, e.g., one-to-one magnification or three-to-one magnification, the inter-frame imaging times, and the attenuation parameters. For these efforts past experience allowed determination of the attenuation parameters, as well as a guide to the time from load-ring to detonator breakout, and then from detonator breakout to the shockwave breakout at the free-surface. Earlier work emphasized the need for the ×3 magnification capability to image ejecta formation and breakup to support ejecta model development efforts. Regarding the specifics of timing, because data on detonation velocities in TNT and PBX 9501 exists, those data were used to estimate the detonation times reasonably accurately. These estimates, together with

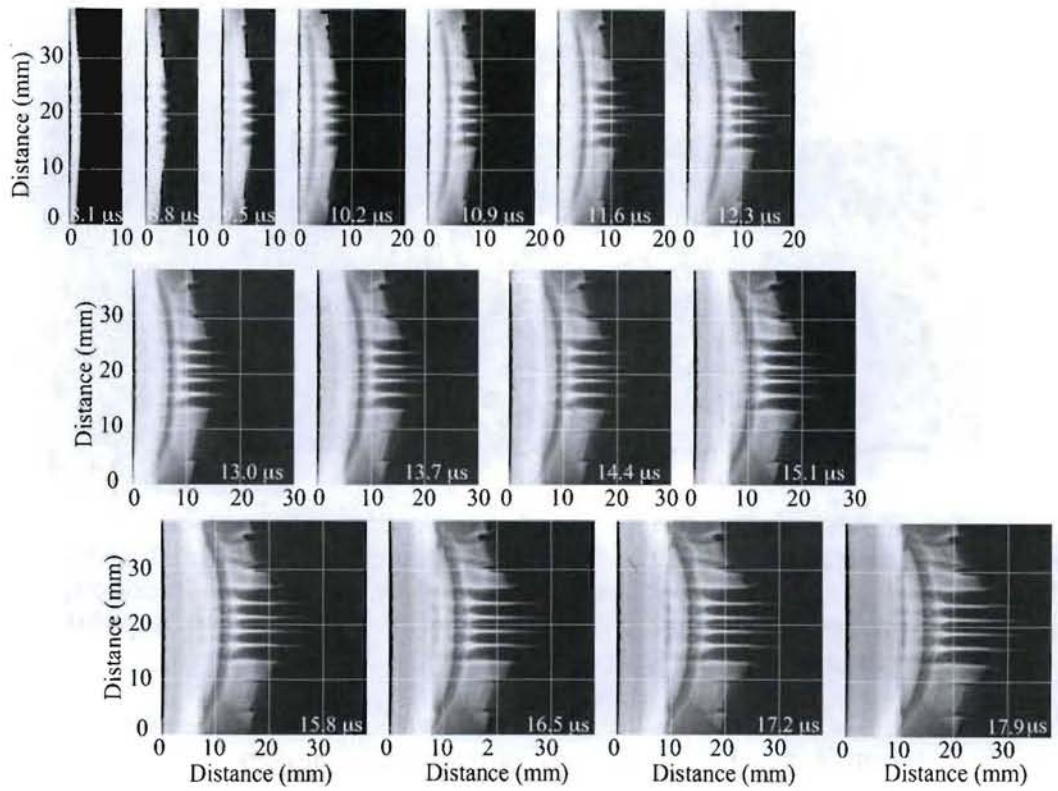

Fig. 4. Images from the FY09 pRad RMI experiments. The time of each image is shown in the lower portion of each image. The instabilities are not fully resolved at this image scale and contrast level. However, the salient features, that include bubble and spike positions relative to the flat regions are evident.

detonator time data, were used to estimate the timing for the images. Because a good estimate of the breakout time is desired, the HE detonation and shockwave velocities were used to predict when the shockwave would release at the Sn/Vacuum or Sn/gas interface, with an expectation of some jitter in this time. To account for timing variation, one exposure was chosen at the estimated breakout time, one exposure 300 ns earlier, and one exposure 300 ns later, to ensure a good estimate of the breakout time. Once the breakout time was in hand, and based on the 40 mm field of view, the expected shockwave pressure P_{SB} in the Sn material just prior to the shockwave release is combined with the ejecta velocity model to estimate the speeds of the fastest ejecta and set the subsequent inter-frame camera times for the vacuum experiment. The ejecta model we are working with is based on a Meyer-Blewett approximation[12] for the fastest ejecta, and it gives estimates for the ejecta "spike" velocities of

$$u_{spk} = u_{fs} + u_{fs}\frac{ka}{2}\left(2 - \frac{u_{fs}}{u_{sh}}\right)$$
$$= u_{fs} + u_{mb},$$

where u_{spk} is the fastest spike velocity, u_{mb} is the Meyer-Blewett velocity, u_{fs} is twice the particle velocity (a.k.a the "free-surface" velocity), ka is the product of the wavenumber and amplitude, and u_{sh} is the velocity of the shockwave within the shocked material, Sn for our purposes. Assuming $P_{SB} \approx 35$ GPa implies $u_{fs} \approx 2.25$ mm/µs and that $u_{sh} \approx 4.27$ mm/µs. Using the largest $ka = 1$ for this system gives $u_{spk} \approx 3.9$ mm/µs. Given that pRad provides 19 high quality images for the ×3 magnifier, that three of those images were grouped early to capture breakout, the remaining sixteen were grouped every 700 ns for the experimental duration.

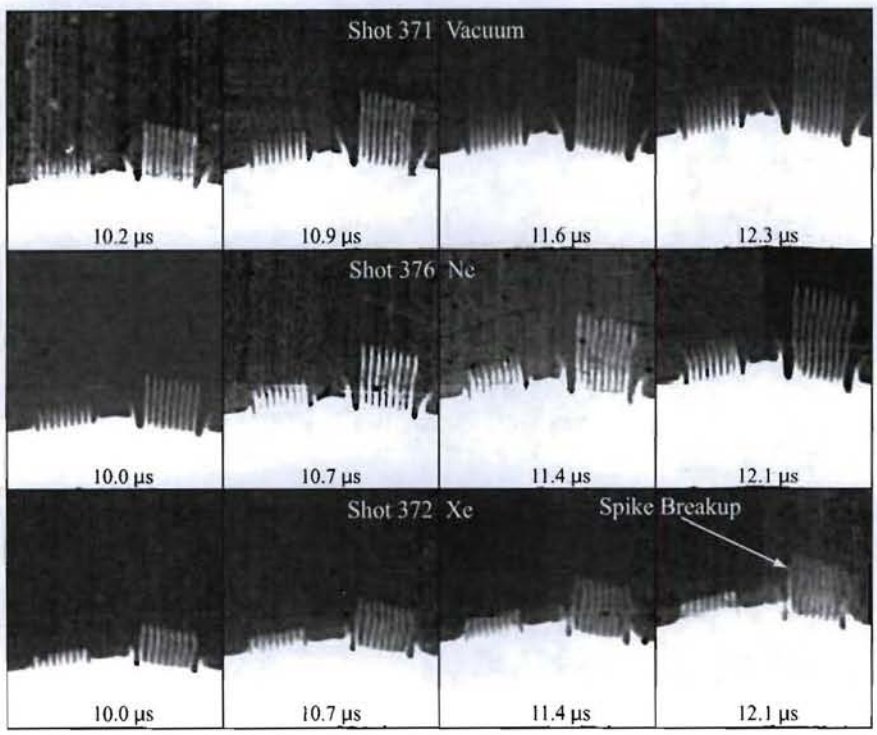

Fig. 5. Vacuum, Ne, and Xe pRad RMI time-series data, beginning just after shockwave breakout, or release. The Sn material is fully liquid on release, and the gas pressure was about 4 atm. for each pressurized experiment. Image times have been matched as well as could be done given that we adjusted the times after the vacuum series.

After the vacuum experiment, we saw that first motion occurred after the third image, so we delayed the timing for the Xe experiment about 200 ns. For the Ne experiment we shifted the timing another 700 ns later. The end result is a good estimate of the timing breakout for all three experiments. Finally, it was observed that $P_{SB} \approx 38$ GPa, higher than expected, a result that will be addressed with a further redesign of our package for FY10 experiments. This also meant that our estimate of u_{spk} was a little low with the better estimate being $u_{spk} \approx$ 4.1 mm/μs. In each case at these shock-loading pressures the Sn is shocked from the beta to bottom-centered-tetragonal phase, and releases to 100% liquid.

These preparations led to the vacuum data presented in Fig. 4. This series of images shows the short-wavelength, large-amplitude ($ka = 1$) RMI spikes travel the fastest, with the short-wavelength and small-amplitude ($ka = 1/4$) traveling at a similar yet lower velocity as the long-wavelength and large amplitude ($ka = 1/4$). The bubbles are also clearly evident and distinguishable from the free-surface (particle) velocity that is determined by the flat regions between the sinusoidal perturbations. Also evident is the decompression of the Sn with time that is denoted in the lower portion of each image.

While every effort was made to create a smooth and continuous interface between the flat regions and the perturbed regions, interface wave effects at the transition between the flat and perturbed regions are nevertheless in evidence. The curvature of the surface increases with time and is exclusively due to late-time release waves scattering within the shocked Sn interface. More desirable would be a completely flat and clean shock release. We will use the hydrodynamic modeling of the packages, as shown in Fig. 3, to inform FY10 experimental packages.

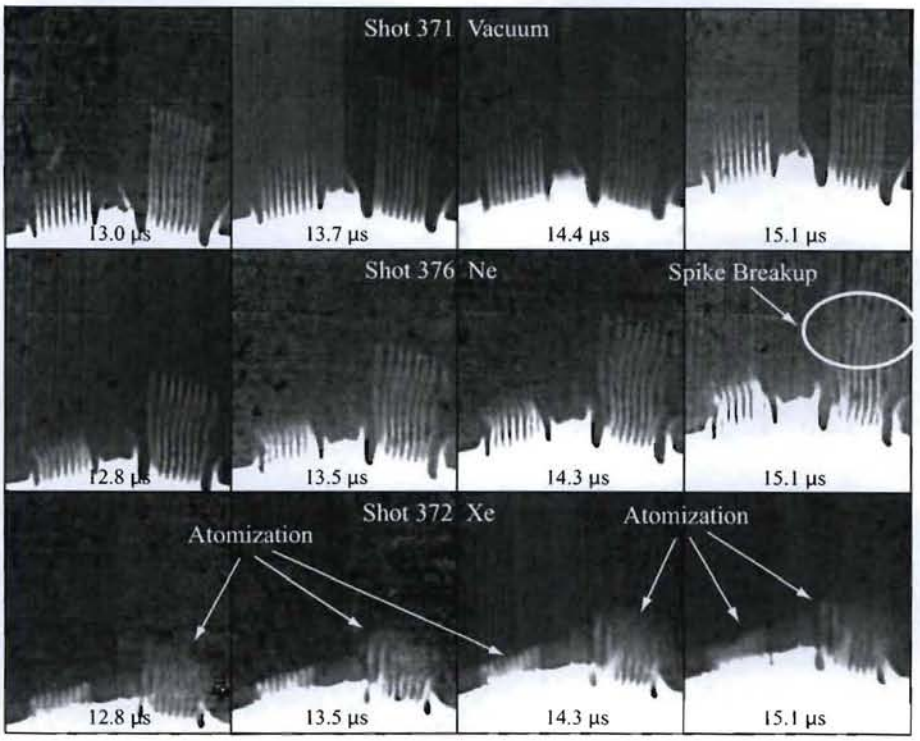

Fig.. 6. Continuation of the vacuum, Ne, and Xe pRad RMI time-series data. Image times have been matched as well as could be done given that we adjusted the times after the vacuum series.

To first order the bubble velocities should be $u_{bbl} \approx u_{fs} - u_{mb}$. In Fig. 4 it is clear that the bubbles are not traveling at the same relative speed to u_{fs} as u_{spk}. This is particularly evident in the long-wavelength region. It is thought that this difference from expectations is due to the fact that the large wavelength is larger than, but on the same order of scale, as the target thickness. We also suspect that the 2 mm Sn thickness is too thin to approximate an infinite well of mass for bubble and spike growth. This is important because the Meyer-Blewett results are based on this assumption. This is likely the cause of the deviation of the bubble velocities from the predictions.

The full time-series data are presented in Figs. 5 to 7. Removed from these data are the long-wavelength regions for reasons mentioned earlier (e.g., $\lambda \approx \tau$), and the $\lambda = 600$ μm regions with $a = 25$ μm and $a = 100$ μm are positioned side-by-side. The flat regions that relate u_{fs} were kept, and the time-stamps, which are relative to detonator-breakout, are included in the bottom of each image and are matched as well as possible to the nearest times of other frames. These images are also adjusted for contrast to reveal where the spike-masses are. Because of this, the bubbles are not perfectly resolved, as can be seen in comparisons with Fig. 4, whose contrast is nominally set to the proton transmission.

From these data it is seen that the RMI spikes in the Ne gas behave much more like the vacuum series than do the RMI spikes in the Xe gas. This is interesting because the viscosity of Ne is about twice the Xe viscosity, i.e., $\eta_{(Ne)} \approx 2\eta_{(Xe)}$. Further, because the density of Xe is about five times the density of Ne, the kinematic viscosity of Ne is about ×10 the kinematic viscosity of Ne: $\eta_{(Ne)}/\rho_{(Ne)} \approx 10\ \eta_{(Xe)}/\rho_{(Xe)}$. The implication is that the Weber number $We = \rho_{Sn} u_{spk}^2 L/\sigma$ dominates the spike-breakup, where L is the spike tip diameter, and σ is the surface tension.

The discussion of particle breakup is important to particle transport in gasses. We have highlighted *We*, but we also observe that hydro models predict that

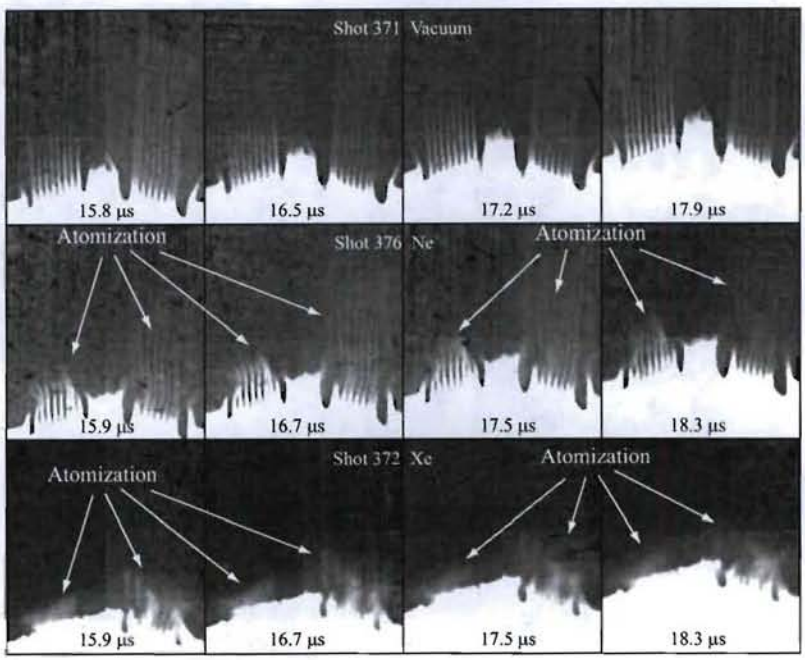

Fig. 7. Continuation of the vacuum, Ne, and Xe pRad RMI time-series data. Image times have been matched as well as could be done given that we adjusted the times after the vacuum series.

the RMI spike tips will not continue to grow thinner with time, but rather that they will become blunted due to surface tension. This effect is nominally seen at around 11.6 μs in the vacuum series, which implies the effect happens in the Ne and Xe series as well, but drag may be stripping liquid Sn off the blunted tips, streaming the material toward adjacent neighbors. This assumption is supported by the fact that the RMI spikes appear to breakup in the middle of the spikes in the Ne gas at time 15.1 μs, and at time 12.1 μs in the Xe gas. Close inspection reveals that there may be some evidence of the mass streaming from the fastest Ne spike tips, in the shape of a mach-stem, to their nearby neighbors at time 11.4 μs.

The vacuum- and Ne-series velocimetry described earlier are presented in Figs. 8 and 9. The Xe velocimetry returned noise, perhaps due to scattering off of the shockwave front. Because of that it is not included in this report.

In Fig. 8 the vaccum jump velocity is seen to be about 2.35 to 2.4 mm/μs on probes 2 and 4 (the flat regions). Also seen in these regions is a small amount of ejecta from the 16 μin. roughness surface. For the region of $ka = 1/4$ (probe 1), the bubble velocity $u_{bbl} \approx 2.2$ mm/μs, and for the region of $ka = 1$ the bubble velocity is $u_{bbl} \approx 2$ mm/μs. Both of these results should be compared with u_{spk} relative to u_{fs}. The spike velocities are also present in the probes 1 and 5 data, and are seen to be $u_{spk} \approx 2.9$ mm/μs for $ka = 1/4$, and $u_{spk} \approx 3.9$ mm/μs for $ka = 1$. Also seen for both the bubble and spike velocities are the non-linear rise times for both regions.

In Fig. 9 the jump velocity in the Ne gas is seen to be about 2.4 to 2.5 mm/μs on probes 2 and 4 (the flat regions), and in these regions the velocity from the small amount of ejecta from the 16 μin. is seen to decrease with time due to breakup and drag, as expected. For the region of $ka = 1/4$ (probe 1), $u_{spk} \approx 2.9$ mm/μs initially, as before, but it quickly attenuates to about 2.3 mm/μs over a time period of about 17 μs. For the region of $ka = 1$, $u_{spk} \approx 3.9$ mm/μs, initially, and it is seen to slow to about 2.7 mm/μs. Also evident in the decreasing ejecta velocities are velocities well below the free surface velocity. This could imply that some mass will be recollected onto the liquid surface. The bubble velocities are not evident in either image, but the

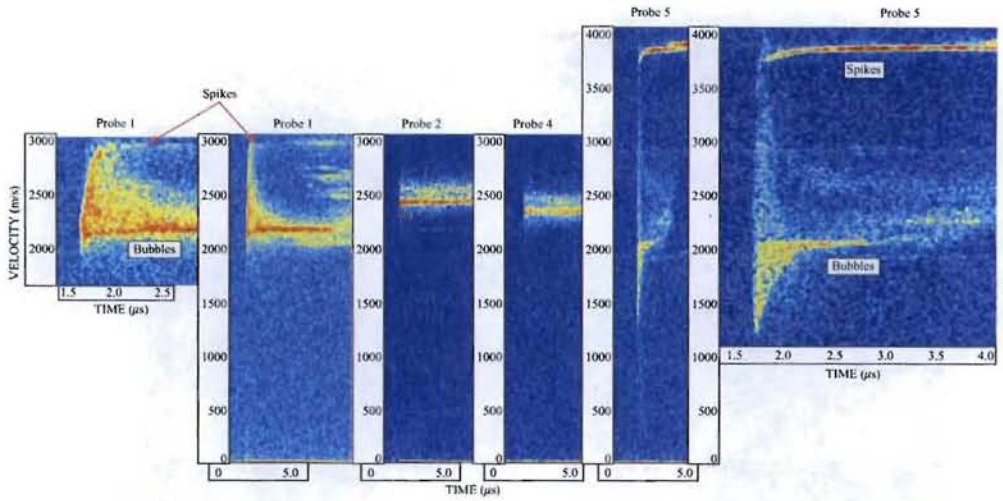

Fig. 8. Vacuum Doppler velocimetry. Probe 1 is in the *ka* = 1/4 region, probe 2 in the adjacent flat region, probe 4 in the next flat region, and probe 5 in the *ka* = 1 region.

proton radiographs show $u_{bbl} \approx 2.0$ mm/μs for the Ne.

For the Xe gas experiment, the proton radiographs were used to estimate $u_{spk} \approx 2.4$, and $u_{bbl} \approx 1.9$ mm/μs for the $ka = 1/4$ region, and in the $ka = 1$ region, $u_{spk} \approx 3.1$ and $u_{bbl} \approx 1.9$ mm/μs. This implies that the inter-frame time of 700 ns is too slow to capture the initial bubble and spike velocities in the gas, but another explanation could be be that the density resolution of pRad is too low to compare with the Doppler velocimetry measurements. In contrast, the free surface velocity reported from the radiographs shows a free surface velocity of $u_{fs} \geq 2.1$ mm/μs, which is lower than the velocity reported by the direct Doppler measurements. This implies that there is a dense layer of ejecta running in front of the surface that the optical measurement cannot penetrate. As noted earlier, the Doppler measurements do show evidence of the ejecta layer at the metal interface that was finished to 16 μin.

In conclusion, these observations can be used for code validation and verification studies. This collection of results will be used to inform FY10 experimental packages and test our working ejecta model. Specifically, it is clear that $\lambda = 2.5$ mm is too long for the ×3 magnifier, and too similar in scale to the coupon thickness. The results also show that $\lambda = 600$ μm is resolvable, and that it is likely that this can be reduced to $\lambda \approx 450$ μm and be resolved. The amplitudes are relevant and need not be changed, but the coupon thickness can be increased to as much as $\tau = 10$ mm. It is also possible to reduce the edge release effects by using a larger diameter booster and lens, especially when combined with momentum trapping concepts that isolate release waves from the central portion of the coupon. Other booster materials, such as PBX 9502 or TNT, can be used to reduce the peak stress, P_{SB}, to levels near 20 GPa, allowing full investigation of other components of our ejecta model development.

Acknowledgments

This work was supported by the United States Department of Energy.

We gratefully acknowledge contributions by Patrick T. Reardon and Machinist Felix P. Garcia of MST-7.

All images were processed by David Oro, Chris Morris, and William Buttler.

The final experiment design was engineered by William Buttler and Guy Dimonte.

Guillermo Terrones did the hydrodynamic modeling of the package.

Finally, the pRad team is extensive, has incredible breadth and talent. Cheers to them all for an outstanding data set. It is likely that someone's name was left off inadvertently. Regrets in advance.

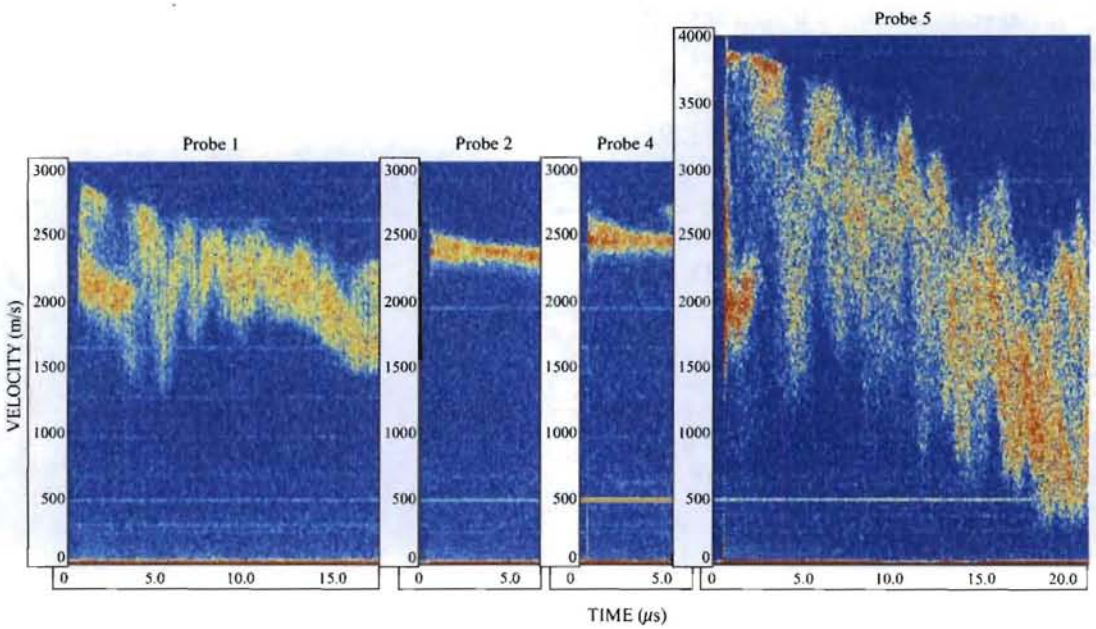

Fig. 9. Ne Doppler velocimetry. Probe 1 is in the *ka* = 1/4 region, probe 2 in the adjacent flat region, probe 4 in the next flat region, and probe 5 in the *ka* = 1 region.

References

1. W. S. Vogan, W. W. Anderson, M. Grover, J. E. Hammerberg, N. S. P. King, S. K. Lamoreaux, G. Macrum, K. B. Morley, P. A. Rigg, G. D. Stevens, D. Turley, L. R. Veeser and W. T. Buttler, "Piezoelectric characterization of ejecta from shocked tin surfaces,"' J. Appl. Phys. **98**, 113508 (2005).

2. W. T. Buttler and S. K. Lamoreaux, "Dynamic chemical effects on reactive metal fragments (U)," Defense Research Review Journal **15**, #1, p. 27-36, Spring (2007).

3. W. T. Buttler, M. B. Zellner, R. T. Olson, P. A. Rigg, R. S. Hixson, J. E. Hammerberg, A. W. Obst, J. R. Payton, A. Iverson, and J. Young, "Dynamic comparisons of piezoelectric ejecta diagnostics," J. Appl. Phys. **101**, 063547 (2007).

4. W. T. Buttler, N. Routley, R. S. Hixson, N. S. P. King, R. T. Olson, P. A. Rigg, A. Rimmer, and M. B. Zellner, "Method to separate and determine the amount of ejecta produced in a second material-fragmentation event," Appl. Phys. Lett. **90**, 151921 (2007).

5. M. B. Zellner, M. Grover, J. E. Hammerberg, R. S. Hixson, A. Iverson, G. Macrum, K. B. Morley, G. Macrum, A. W. Obst, R. T. Olson, J. R. Payton, P. Rigg, N. Routley, G. Stevens, D. Turley, L. Veeser and W. T. Buttler, "Effects of shockbreakout pressure on ejection of material from shocked tin surfaces," J. Appl. Phys. **102**, 013522 (2007).

6. W. T. Buttler and M. B. Zellner, "Tin ejecta data review: toward a statistical material fragmentation model, Milestone 2478," Los Alamos National Laboratory internal publication, LA-UR-07-6522 (2007).

7. M. B. Zellner, W. Vogan-McNeil, G. T. Gray, III, D. C. Huerta, N. S. P. King, G. E. Neal, S. J. Valentine, J. R. Payton, J. Rubin, G. D. Stevens, W. D. Turley and W. T. Buttler, "Surface preparation methods to enhance dynamic surface property measurements of shocked metal surfaces," J. Appl. Phys. **103**, 083521 (2008).

8. M. B. Zellner, M. Grover, J. E. Hammerberg, R. S. Hixson, A. Iverson, G. Macrum, K. B. Morley, A. W. Obst, R. T. Olson, J. R. Payton, P. Rigg, N. Routley, G. Stevens, D. Turley, L. Veeser and W. T. Buttler, Erratum: "Effects of shock-breakout pressure

on ejection of material from shocked tin surfaces," [J. Appl. Phys. {\bf 102}, 013522 (2007)], J. Appl. Phys. **103**, 109901 (2008).

9. M. B. Zellner, M. Grover, J. E. Hammerberg, R. S. Hixson, A. W. Obst, R. T. Olson, J. R. Payton, P. Rigg, N. Routley, G. Stevens, D. Turley, W. Vogan-McNeil, and W. T. Buttler, "Probing the underlying physics of ejecta production," J. Appl. Phys. **103**, 123502 (2008).

10. R. D. Richtmyer, Commun. Pure Appl. Math **13**, 297 (1960).

11. E. E. Meshkov, Izv. Akad. Nauk SSSR, Mekh. Zhidk. Gasa **4**, 151 (1969) [Izf. Acad. Sci. USSR Fluid Dynamics **4**, 101 (1969)].

12. K. A. Meyer and P. J. Blewett, Phys. Fluids **15**, 753 (1972).

13. The Sn samples are shocked along the Hugoniot to pressures where the Sn shocks from the solid β to the solid bottom-centered-tetragonal (BCT) phase that then releases to mixed solid-liquid phase

14. C. A. Forest, R. L. Rabie, L. Bennet, and J. Vorthman, ``A novel explosively driven flying plate system," in *Proceedings of the 11th International Detonation Symposium*, Snowmass, CO. August 31 to September 4, 1998.

15. The FY08 experiments were supported shockwave experiments as the shockwave was caused by a flyer plate. The small scale HE experiments, and our FY09 results, are unsupported, or Taylor, shockwave loading experiments.